Biosensors and Bioelectronics 146 (2019) 111740

Contents lists available at ScienceDirect

Biosensors and Bioelectronics

journal homepage: http://www.elsevier.com/locate/bios

Nanopore biphasic-pulse biosensor

Hong Sun [1], Fujun Yao [1], Xiao-Feng Kang [*]

Key Laboratory of Synthetic and Natural Functional Molecular Chemistry, College of Chemistry & Materials Science, Northwest University, Xi'an, 710069, PR China

ARTICLE INFO

Keywords:
Nanopore
Biphasic pulses
Lysozyme
Protein detection
Nanodevice

ABSTRACT

Nanopores as artificial biomimetic nanodevices are of great importance for their applications in biosensing, nanomedicine and bioelectronics. However, it remains a challenge to detect small biomolecules especially small-sized proteins with high sensitivity and selectivity. In the article, we report a simple and efficient method for small-sized protein detection by constructing biphasic-pulse nanopore biosensor. Unlike the traditional resistive pulse sensing, the biphasic-pulse event can provide unique and abundant fingerprint information. Although the nanopore biphasic-pulse electrical signal is originated from both the molecular exclusion electrical resistance and the surface-charged effect of confined molecule, its frequency and amplitude of the waveform can be adjusted by pH, applied potential and salt concentration. Based on the frequency of the biphasic pulse, nanomolar concentration of proteins could be specifically detected and the limit of detection is 1.2 nM. In addition, the biphasic-pulse nanopore shows well discrimination in similar-sized protein detection and its signal generation is highly reproducible. The nanopore biphasic-pulse biosensor should have broad applications as a new generation of powerful single-molecule device.

1. Introduction

Biological cells, tissues and organs are natural molecular devices of nanostructure units by which physiological processes and activities are implemented and modulated. For instance, biological nanochannels or nanopores assembled by membrane-spanning proteins can intelligently communicate and regulate ions/molecules as well as energy inside and outside the cells (Manrao et al., 2012; Zhou et al., 2001). The opening or closing of nanochannels can be controlled by various of physiological stimulus (acidity, temperature, light, voltage and metabolites etc.), which in turn regulated the flux of ions/molecules across membranes, resulting in the generation of electrical signals (Ding et al., 2019). The heart in the body is another example. Both atria and ventricles work together, alternately contracting and relaxing to pump blood molecules through heart vascular. The electrical system of heart is a power source that makes the function possible. Inspired by natural molecular devices, designing and developing biomimetic nanodevices, such as single-molecule detector are urgently demanded.

Nanochannels/nanopores including those of nature and artificialness have been developed as molecular devices for analytical detection (Ying et al., 2018; Yu et al., 2019), DNA sequencing (Farimani et al., 2017; Garaj et al., 2010), biomolecular interaction (Fanzio et al., 2015; Kwak et al., 2016; Thakur and Movileanu, 2019), chiral and conformation analysis (Kang et al., 2006; Van Meervelt et al., 2017). However, all of the nanodevices are fully based on the simple single-peak current pulse signals produced by molecules-blocking events. The simple signatures are insufficient to acquire their unique and abundant fingerprint information.

To develop portable nanodevices, artificial solid nanopore/nanochannel has several advantages compared with lipid-based systems, such as adjustable geometry and size, superior mechanical, chemical and thermal characteristics, addressable functionalities on the surface and the easy of integrating with electronic or optical readout techniques (Xiao et al., 2016). The basic sensing principle is that an applied potential drives the analyte molecule through the nanopore, thereby inducing characteristic temporary changes in the nanopore ionic current which serve as "fingerprints" of the translocating molecules. The amplitude, duration and frequency of current pulse can reflect the information of size, charged status and the concentration of the analyte. The single-peak electronic pulse signals for various kinds of artificial nanopores can be also modulated by environmental inputs such as ions (Wei et al., 2018), pH (Anderson et al., 2013), temperature (Arnott and Howorka, 2019), light (Verschueren et al., 2019) and voltage (Siwy and Howorka, 2010), although weak electrical signals with lower

* Corresponding author.
E-mail address: kangxf@nwu.edu.cn (X.-F. Kang).
[1] These authors contributed equally to this work.

https://doi.org/10.1016/j.bios.2019.111740
Received 9 July 2019; Received in revised form 24 September 2019; Accepted 27 September 2019
Available online 28 September 2019

signal-to-noise ratio and weak interaction between analyte and inner wall of nanochannel. Furthermore, we note that the electrical pulse signals of nanopores are generally current blockage (Bayley and Martin, 2000; Houghtaling et al., 2018) and a few existed as conductance increase which can be attributed to the excess ions that the analyte brings into the pore during translocation (Chang et al., 2004; Smeets et al., 2006). Nevertheless, for those single-peak signals, the analysis of target molecule is easily interfered by complex components in biological samples due to the limited feedback information. Constructing biphasic-pulse or even multiple-peak signals and comprehensive consideration of their producing mechanism may reflect more size and charge information for the benefit of specific discrimination of analyte.

The electronic signals in the human body are complex and diverse. Heart rhythms are biphasic pulses waveshape signal, rather than monophasic pulses. Monitoring, simulating and constructing these signals and developing implantable electronic devices (IED) based on them are of great significance for human being (Feiner and Dvir, 2018). IED, such as intelligent gastric and cardiac pacemakers, cochlear implants and deep brain stimulators (Cheng and Tereshchenko, 2011) can be used for recording electrophysiological signals and stimulating muscles and nerves in clinical medicine (Kim et al., 2016) and now they are becoming widely used crucial medical technologies for monitoring, measuring and soliciting physiological responses in vivo (Zheng et al., 2016). For instance, the implantable cardioverter defibrillator (ICD) with biphasic waveform (as shown in Fig. 1a top) is highly effective to significantly decrease the energy level necessary for successful defibrillation (Mossesso et al., 2011), thus decreasing the risk of burns and myocardial damage (Migliore et al., 2019). To extend the application of IED, more precise biological electronic devices are burgeoning. One of the important directions is constructing biomimetic nanodevices that can realize the real-time detection of the specific protein and prediction of the protein-related diseases.

In this work, we report an artificial biomimetic biphasic-pulse nanopore device. The biphasic waveshape signal was produced by a specially designed polymer nanopore with unique three-dimensional structure and size. The emphasis of the paper lies on (1) how to generate distinct biphasic waveshapes using the conical nanopore and its forming mechanism; (2) how to adjust and control the characteristics of the biphasic-pulse signals such as frequency, amplitude and the resolution of event signals. Moreover, we show its sensing application in analytical detection, displaying high sensitivity and selectivity. To demonstrate the feasibility of our method, lysozyme, a small-sized protein (dimensions $4.5 \times 3.0 \times 3.0$ nm, molecular weight 14.3 kDa) was chosen as the target model. It has been reported that lysozyme plays an important role in the immune system of the human body with the abilities of antibacterial activity and has other applications like drug delivery and tumour marker (Haselberg et al., 2011; Rezaei et al., 2018). Our experimental results showed that neat and orderly biphasic-pulse signals were observed during lysozyme translocation across the nanopore. The method had successfully overcome the challenge of the

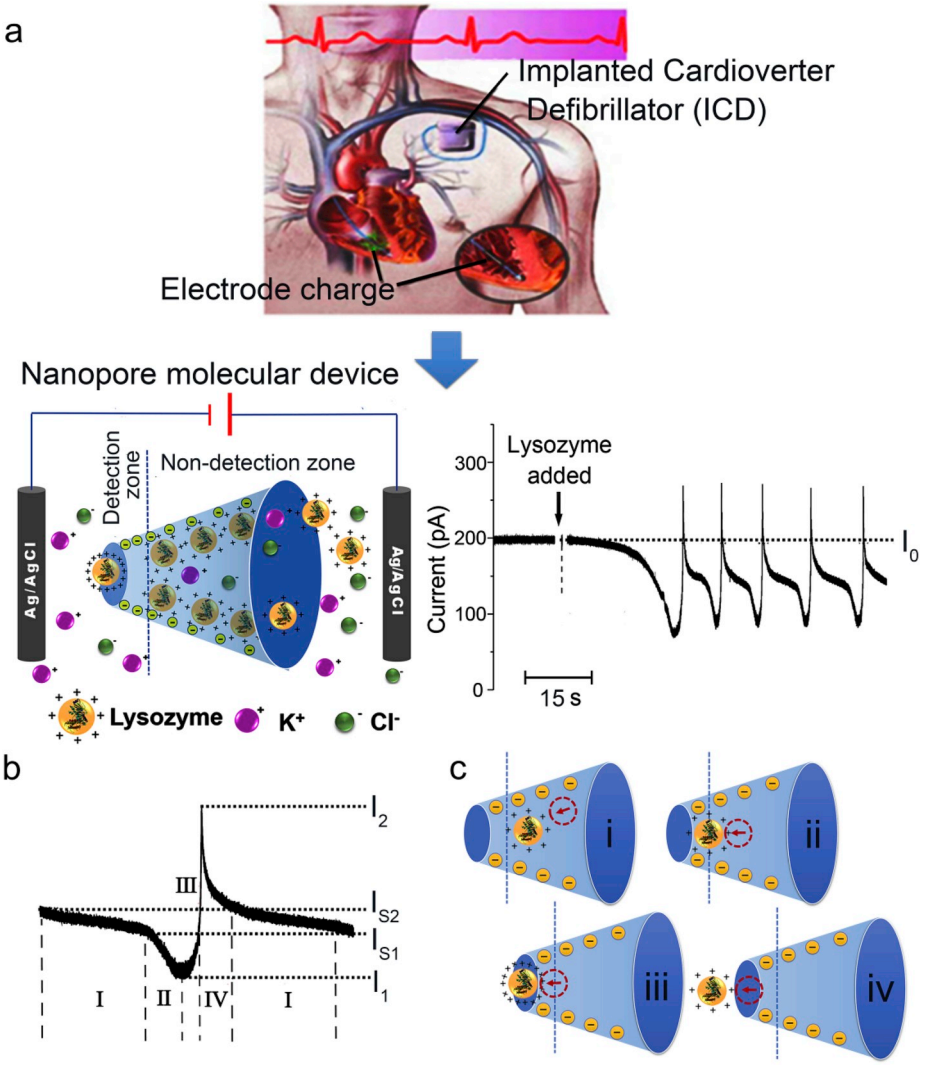

Fig. 1. The design of nanopore biphasic-pulse nanodevice and application for lysozyme sensing. (a) Schematics of the implantable cardioverter defibrillator (ICD) with biphasic-pulses waveform (top), the transport of lysozyme molecules through the nanodevice (bottom left) and representative biphasic-pulse current trace corresponding to 100 nM lysozyme translocation (bottom right). Experimental conditions: 100 mM KCl buffered with 10 mM Tris (pH 7.0), with transmembrane potential of +1000 mV. (b) Expanded view of a typical biphasic-pulse event of single lysozyme molecule in the panel a. (c) Diagrammatic drawing of the translocation process corresponding to the segments of I, II, III and IV denoted in b. The sensing zone and the non-detection zone in conical pore were separated by a vertical line.

small-sized protein sensing, which is much difficult to be realized due to its fast translocation and low sensitivity in nanopore sensors (Lin et al., 2017). The developed single-molecule artificial biphasic-pulse nanopore device could also have powerful potential in detection of other biomolecules.

2. Experimental section

2.1. Materials and regents

Poly (ethylene terephthalate) (PET) membranes (12 μm in thick), which contained a potential track irradiated by a single heavy-ion (Au) with energy of 11.4 MeV per nucleon, were purchased from GSI (Darmstadt, Germany). Lysozyme (L6876) and Trypsin (T7409) were bought from Sigma-Aldrich. All other reagents were of analytical grade and used as received.

2.2. Fabrication and characterization of nanochannel

The asymmetric structure and the carboxylate groups (p*Ka* ~3.8) on the inner surface of nanochannel are generated after etching. When the pH was above the p*Ka*, the carboxylate groups were deprotonated and the nanochannel became negatively charged. The prepared conical nanochannel has two openings. The diameter of the large opening (terms as the base) was approximately 400 nm (Fig. S1a), which was measured by scanning electron microscopy (SEM, Hitachi S-4800, Japan). The diameter of small opening (terms as the tip) was calculated to be ~6 nm through electrochemical measurements (Fig. S1b). (The details fabrication and characterization of nanochannel see the Supporting Information).

2.3. Lysozyme translocation experiment

The conical polymeric nanochannel separated the cells into two isolated containers. The tip side of the nanochannel acted as the cis reservoir (connected to "ground"), while the base side acted as the trans reservoir. Both containers were filled with 100 mM KCl (10 mM Tris-HCl, pH 7.0). For the lysozyme transport experiment, the buffered fresh lysozyme solution was added to the base side, a positive voltage of +1000 mV was used to drive the positively charged lysozyme passing through the nanochannel from the base to tip. A patch clamp amplifier (Axopatch 200B, Molecular Devices Inc.) was employed to measure and synchronously record the current trace across the conical nanochannel. The current data were filtered by a low-pass Bessel filter of 5 kHz, sampled at 20 kHz by a computer equipped with a Digidata 1550 converter (Molecular Devices). The schematic diagram of the entire instrument system is shown in Fig. S2. The event amplitude and duration were analysed by using Clampfit 10.5 (Molecular Devices) and origin 9.0 (Microcal, Northampton, MA) software (details data analysis see the Supporting Information).

3. Results and discussion

3.1. Nanopore biphasic-pulse signatures

According to our preliminary experiments, three vital factors had to be considered for constructing distinctive biphasic pulses-based nanopore: the molecular migration rate in nanochannel, the molecular exclusion electronic resistance and the conductivity of confined molecule. The molecule migration rate in nanochannel is slowed down to facilitate the formation of the biphasic pulse signal. We thus designed a conical polymeric nanopore with a nanometer-sized orifice tip, whose diameter was comparable to the molecular size of the channel and selected the inner wall of the polymer that is opposite in charge to the channel molecule. The combination of the space effect and the electrostatic effect could provide effective molecular moving resistance. In addition, the translocating molecule in filled-salt nanopore can produce an exclusion electronic resistance, which results in the decrease of ionic current. However, the ionic current is also likely to increase through electrical gating of surface charge in the channel due to the charge of translocating molecule itself (Chang et al., 2004; Smeets et al., 2006). The behaviour of the translocating molecule in the nanopore with special shape could be different at various translocating stages. It is possible to obtain biphasic waveshape signal in the conical nanopore by precisely regulating and balancing the pore-molecule interaction and surface charge effect.

Based on this design concept, we prepared the conical poly (ethylene terephthalate) (PET) nanopore (Fig. 1a, bottom left) by the asymmetry ion track etching technique. The prepared conical nanochannel has two openings, the diameter of the large opening (terms as the base) was approximately 400 nm (Fig. S1a) observed from scanning electron microscopy. The diameter of small opening (terms as the tip) was measured to be ~6 nm through electrochemical method (Fig. S1b). Here, we chose lysozyme as a translocating molecule. Recordings were made in 100 mM KCl, buffered with 10 mM Tris (pH 7.0), at an applied potential of +1000 mV (base side). As expected, a series of biphasic pulses were observed in the current-time traces, which included both resistive and conductive components (Fig. 1a, bottom right). By a close examination of each single event signal, we found that the ionic current through the nanochannel initially experiences a slow decrease and then a rapid increase to a value that is ~72.5 pA higher than the baseline current ($I_0 = 190 \pm 6$ pA). To confirm that the biphasic pulse characteristic signals were yielded by the translocation of the lysozyme molecules, a control experiment was carried out in the absence of lysozyme. Only a relatively steady baseline current can be observed (Fig. 1a, bottom right). In addition, when adding 100 nM lysozyme to the tip side reservoir, no pulse signal was observed at negative potential of -1000 mV (Fig. S3). A possible explanation could be that owing to the lack of preliminary velocity slowness derived from the electrostatic interaction, the lysozyme would translocate with a fast speed at the tip where the field strength strongly focused, which may be beyond the temporal resolution of the instruments (Harrell et al., 2006).

To gain insights into the formation mechanism of biphasic pulse, a typical signature for single lysozyme molecule translocation was shown and divided into four stages, denoted as partI, part II, part III and part IV, respectively (Fig. 1b). As shown in Fig. 1c, the illustrations of translocation processes (i-iv) are separately corresponded to the different segments (I-IV) of biphasic-pulse ionic current signal. PartI is corresponding to the adsorption of proteins on the pore wall through the pore-protein electrostatic interaction (Fig. 1c–i). With the lysozyme molecule moving toward the pore orifice (Fig. 1c-ii), the volume exclusion initially played a dominant role and the resistive pulse was observed. When the lysozyme molecule was in close proximity to the pore orifice (Fig. 1c-iii), the molecular surface charge effect would be more pronounce since the electric field across the conical-shaped pore was highly confined at the orifice (Sexton et al., 2010). Thus, the current increased dramatically at the pore orifice because surface charge effect exceeded the volume exclusion effect. In stage iv, the lysozyme molecule desorbed, left the nanopore (Fig. 1c-iv), and the current finally went back to the baseline. During whole recording, the baseline current and biphasic pulse signals including frequency and amplitude were quite steady, reflecting good reproducibility.

We further analysed the details of the biphasic pulse signal and proved the mechanism. With a lysozyme molecule entering in the sensing zone (usually the first ~1 μm zone from the tip) (Sexton et al., 2010), the current gradually decayed from Is_2 to Is_1 (Is_2 and Is_1 are the initial and the final current values of part Iin Fig. 1b, respectively). Then, the current continued to decrease to the value I_1 until a sudden rise to the value I_2 that was much higher than the baseline I_0, as shown in part II and III (Fig. 1b). The current decrease was probably due to the volume exclusion effect, while the current increase was attribute to the contribution of surface charge effect from the high concentration of mobile

counterions and the highly charged lysozyme molecules. This phenomenon was supported by previous reports in a few DNA translocation experiments (Chang et al., 2004; Smeets et al., 2006). In part IV, when the lysozyme molecule desorbed and left the nanopore, a rapid exponential current decaying occurred due to the ion redistribution process associated with electric double layer and the current thus decreased to the value I_{s1} (Fig. 1b). The above four segments constituted a whole translocation process for an individual event, and the subsequent events would repeat this process one by one. When each translocation process completed, the current returned to the new steady state, as shown in part I (Fig. 1b). Note that the current values of I_1, I_{s1}, I_{s2} and I_2 were all referenced to the background current of I_0, so I_1, I_{s1}, I_{s2} was negative in our discussion.

Next, the statistical analysis of a total of 420 translocation events was done to better understand the mechanism of 200 nM lysozyme translocation through the nanochannel (Fig. 2a). The translocation events of lysozyme were analysed to determine the dwell time (τ) and the conductance change (ΔI_1 and ΔI_2 represent the amplitude of current drop and current rise, respectively). Fig. 2b showed the scatter plots of ΔI_1 (red) and ΔI_2 (green) versus characteristic time τ_1 and τ_2, respectively. Fitting $\Delta I_1/I_0$ and $\Delta I_2/I_0$ histograms to Gauss function, yielded mean values of $\Delta I_1/I_0 = 0.436 \pm 0.013$ and $\Delta I_2/I_0 = 0.375 \pm 0.015$, respectively, as displayed in Fig. 2c τ_{on}, τ_1, τ_2 and τ_3 illustrated in Fig. 2d corresponded the dwell time of the four processes (part I, II, III and IV in Fig. 1b) during lysozyme translocation and we found that τ_1, τ_2 and τ_3 were all well fitted with exponential decay functions. The exponentially varying behaviour revealed that the three parts (parts II, III and IV) should be related to some transient relaxation processes (Wang et al., 2015). The normalized histograms of τ_{on}, τ_1, τ_2 and τ_3 were plotted in Fig. 2e–h, and each histogram was fitted into the Gaussian distribution, with the mean fitted characteristic values of 3.870 ± 0.060, 0.570 ± 0.002 s, 0.080 ± 0.001 s and 0.170 ± 0.001 s, separately.

3.2. Regulation of nanopore biphasic-pulse signatures

pH value of the electrolyte is known to have a significant influence on the translocation behaviour of biomolecules, since the surface charge density of the nanochannel and charged properties of biomolecules can be finely tuned by modulating the pH (Steinbock et al., 2014). As shown in Fig. 3a, for pH 7.0, pH 8.0 and pH 9.0, well defined biphasic pulses were generated in the current traces. By statistical analysis of a total of 280 translocation events, the normalized current drop ($\Delta I_1/I_0$) and rise ($\Delta I_2/I_0$) increased with the pH values decreasing from 9.0 to 7.0 (Fig. 3b). We attributed this phenomenon to the surface charge effect of lysozyme and nanochannel. The lysozyme molecule (isoelectric point, pI 11.0) is positively charged when pH < 11.0 (Lin et al., 2017) and the inner wall of nanochannel was negatively charged at pH > 3.8 owing to the deprotonation of –COOH groups (pKa ~3.8) (Zhao et al., 2013). Therefore, the net charge of lysozyme increases (Yadav et al., 2017) while the surface charge density of the inner wall decreases when pH varying from 9.0 to 7.0 (Fig. S4). The lysozyme in the nanochannel initially induces the effect of concentration polarization and a depletion zone was formed in the front of the passing lysozyme molecules. It is the depletion zone that enhances the current drop beyond a level produced by the volume exclusion of the lysozyme. Since more highly charged lysozymes cause stronger effect of concentration polarization, accordingly increases the extent of the depletion zone, generating an increased $\Delta I_1/I_0$ (Qiu et al., 2016a). As a result, a noticeable increase of the $\Delta I_1/I_0$ would be observed as the pH changed from 9.0 to 7.0. When the lysozyme molecule was in close proximity to the pore orifice, the excess

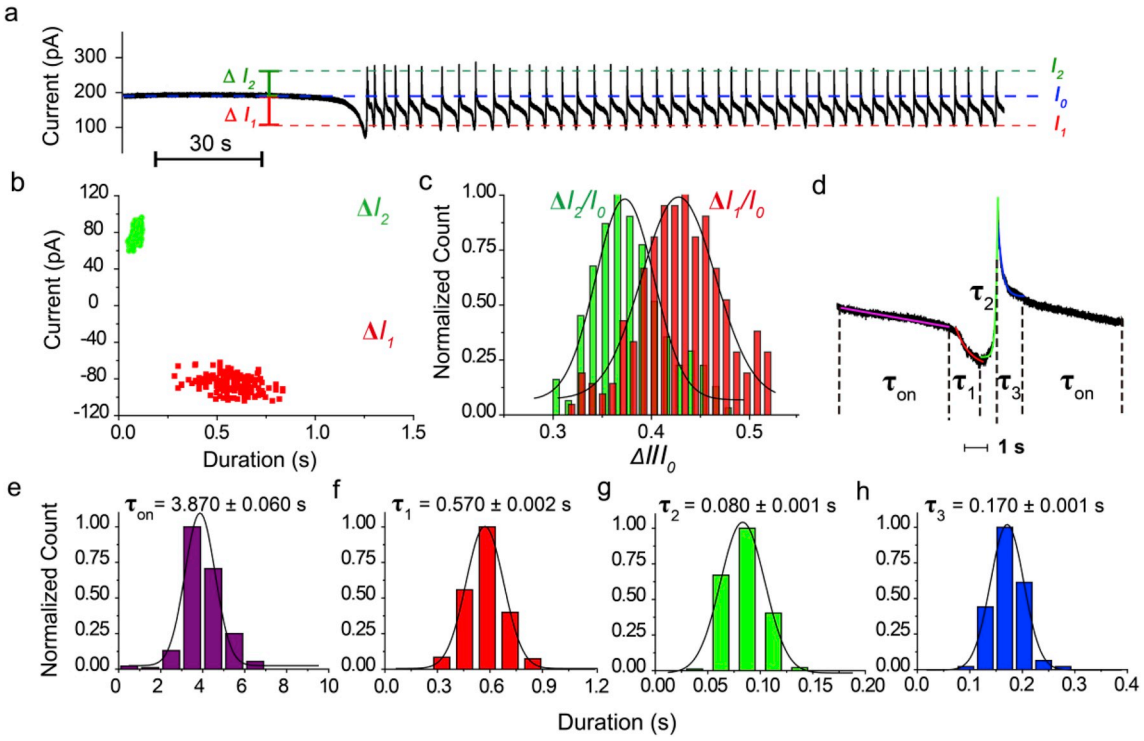

Fig. 2. The analysis of lysozyme translocation based on biphasic-pulse events. (a) The current trace upon adding buffered 200 nM lysozyme solution to the base side of conical nanochannel. (b) The scatter plot of current amplitude versus dwell time for each individual biphasic pluses event. The red color is the current drop, while the green color is the current rise. (c) Normalized histogram of the current amplitudes for downward ($\Delta I_1/I_0$) and upward ($\Delta I_2/I_0$) of a total of 420 translocation events, respectively. (d) Expanded view of a typical single biphasic pluses event indicated in the panel Fig. 2a, in which τ_{on}, τ_1,τ_2 and τ_3 correspond to the duration in part I, part II, part III and part IV as described in Fig. 1b, τ_1 (red), τ_2 (green) and τ_3 (blue) were all well fitted with exponential decay functions, respectively. (e) (f), (g) and (h) are the normalized histograms of event duration, the mean fitted values of τ_{on}, τ_1, τ_2 and τ_3 were 3.870 ± 0.060 s, 0.570 ± 0.002 s, 0.080 ± 0.001 s and 0.170 ± 0.001 s, respectively. Experimental conditions: 100 mM KCl buffered with 10 mM Tris-HCl (pH = 7.0), with a transmembrane potential of +1000 mV. (For interpretation of the references to color in this figure legend, the reader is referred to the Web version of this article.)

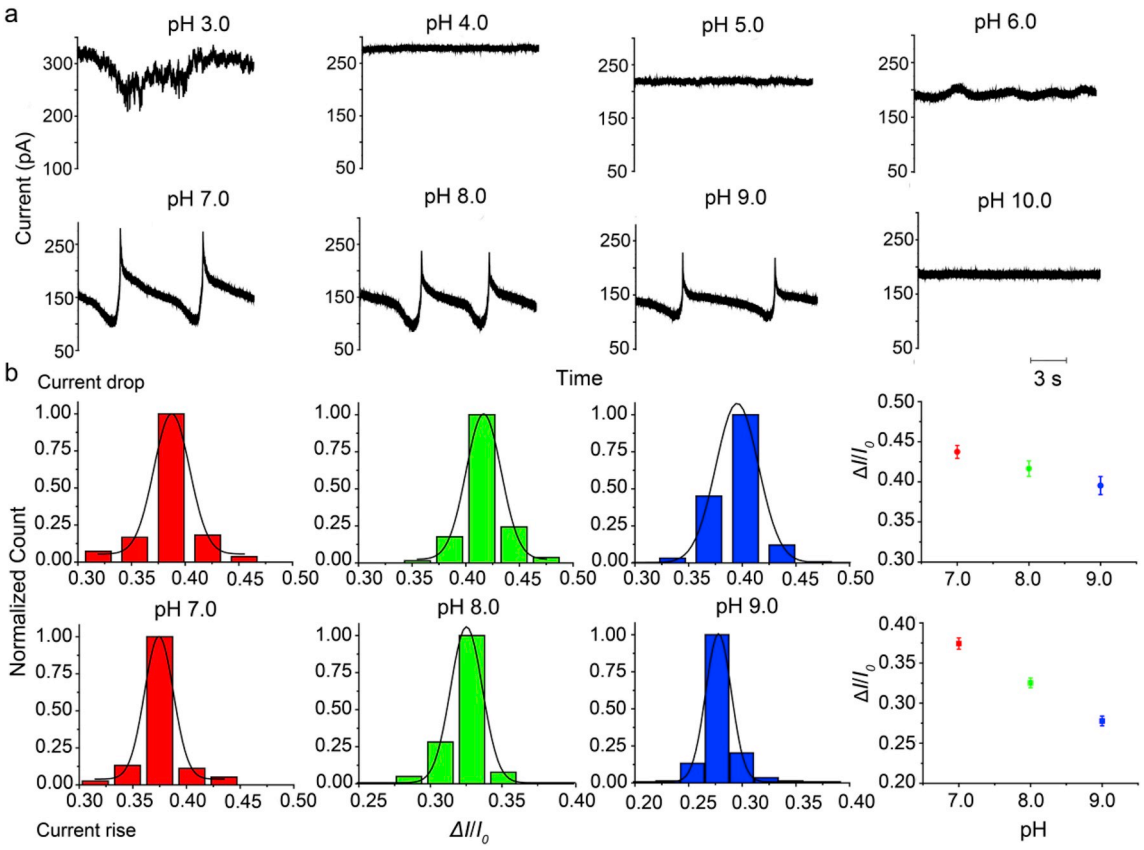

Fig. 3. (a) Typical current-time traces of lysozyme (100 nM) translocation at different electrolyte pH (3.0–10.0). (b) The normalized histograms of current drop ($\Delta I_1/I_0$) and current rise ($\Delta I_2/I_0$) of a total of 280 translocation events at pH 7.0 (red), 8.0 (green) and 9.0 (blue), respectively. Experimental conditions: 100 mM KCl buffered with 10 mM Tris-HCl, with a transmembrane potential of +1000 mV. (For interpretation of the references to color in this figure legend, the reader is referred to the Web version of this article.)

mobile counterions that the lysozyme brings into the pore during translocation are responsible for the current increase. More counterions would be introduced into the nanochannel because of an increase in the charge of lysozyme molecule, thus the $\Delta I_2/I_0$ value would increase with the pH varying from 9.0 to 7.0. Therefore, the highly charged proteins would make the biphasic pulse much evident, especially for the $\Delta I_2/I_0$. On the other hand, the surface charge of the nanochannel also influences the signals (Lan et al., 2014). Although the net charge of lysozyme is weakened at pH 9.0, the waveshape of biphasic-pulse is still obvious (Fig. 3a). These findings implied that the more highly charged of nanochannel, the more evident of the current increase component. Our results are consistent with previous study which attributed the nanopore current rise to the increasement of the surface charge density of nanochannel (Chen et al., 2015; Lan et al., 2014).

However, when the pH value decreased to 6.0, only a few fluctuations with small amplitudes appeared at the current trace and the translocation events could hardly be identified. This is probably due to the stronger electrical field driving force toward the lysozyme derived from the increase in its net charge, which make the protein translocation occur on an extremely short time scale. Thus, translocation events cannot be effectively captured since the time-resolved signal is beyond the resolution of measurement instruments. Moreover, with the pH value decreased to 5.0 and 4.0, the faster translocation velocity of lysozyme, which resulted from the more net charge, leading to no characteristic signals being detected. To verify our explanation, we further investigated the translocation of lysozyme using a higher filter and sampling frequency with the Axopatch 200B amplifier and the Digidata 1550 converter. The current data were filtered by a low-pass Bessel filter of 100 kHz, sampled at 500 kHz (Fig. S5), no translocation event signal was detected. When the pH decreased to 3.0, irregular long-time blocking pulse signals were generated with the translocation of protein. A possible reason would be that the surface charge property of the inner wall of nanochannel was changed from negative to positive at pH 3.0 (Dong et al., 2019) and the original electrostatic attraction between proteins and pore was reversed to electrostatic repulsion. Thus, the irregular long-time blocking pulses may be numbers of lysozyme molecules continuously transport through the nanochannel. As the pH increased to 10.0, an experimental phenomenon similar to pH 4.0 was observed. This was probably because that the weak charged lysozyme cannot translocate though the nanochannel at this pH. Comparing the translocation behaviour at different pH values, we speculate that the protein-nanochannel interactions might play an important role to the biphasic pulses.

To characterize the effect of applied voltage on the shape of biphasic pulse, the translocation of lysozyme molecules was further investigated at different voltages, ranging from +1000 mV to +700 mV (Fig. 4a). As the voltage was decreased to +900 mV, the shape of the biphasic pulses remained unchanged, however, the normalized current conductive $\Delta I_2/I_0$ and resistive $\Delta I_1/I_0$ components were decreased. In addition, the time interval and dwell time of events are prolonged. When the voltage was decreased to +800 mV, the characteristic biphasic pulses were severely weakened, the increased conductance ΔI_2 remained only 5.22 ± 0.32 pA. Finally, no translocation signal was observed when the voltage was further decreased to +700 mV.

By statistical analysis of a total of 248 translocation events, the $\Delta I_1/I_0$ and $\Delta I_2/I_0$ were both enhanced with the voltage increasing (Fig. 4b and c), and the normalized histograms for $\Delta I_1/I_0$ and $\Delta I_2/I_0$ were shown in Figs. S6a and b. The effect of voltage on the $\Delta I_2/I_0$ can be attributed to the surface charge effect of the lysozyme molecule and nanochannel. Previous studies revealed that surface charge effects of the translocating

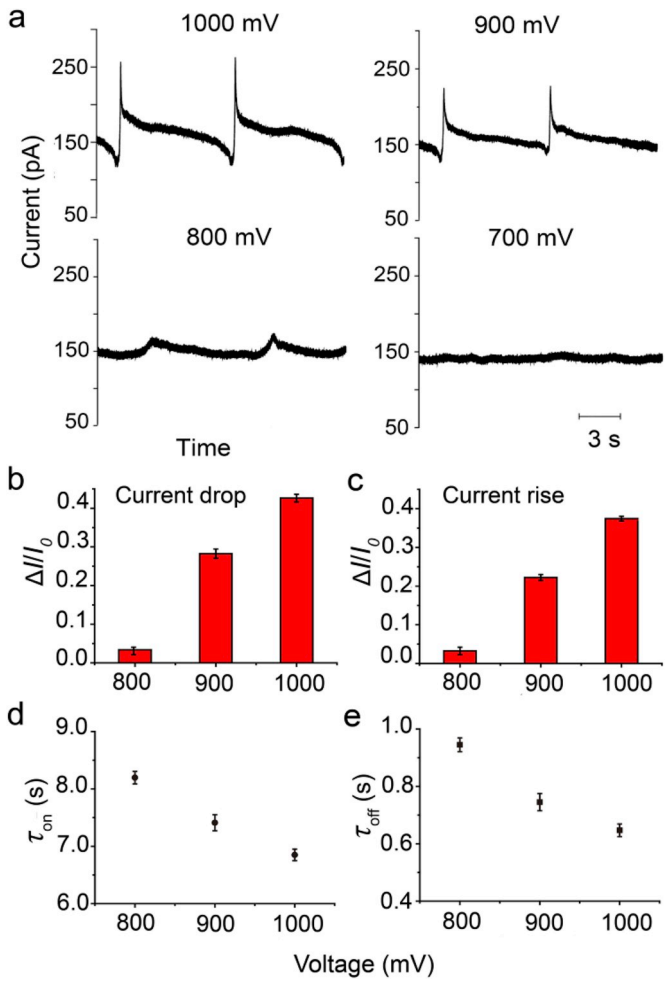

Fig. 4. (a) Representative translocation events of lysozyme molecule (100 nM) at various voltages (700 mV–1000 mV). Effect of the applied potential bias on the current drop (b) and current rise (c). Effect of the applied potential bias on the interval times (d) and dwell times (e) of individual biphasic pulse event of a total of 248 translocation events. Experimental conditions: 100 mM KCl buffered with 10 mM Tris-HCl (pH 7.0) .

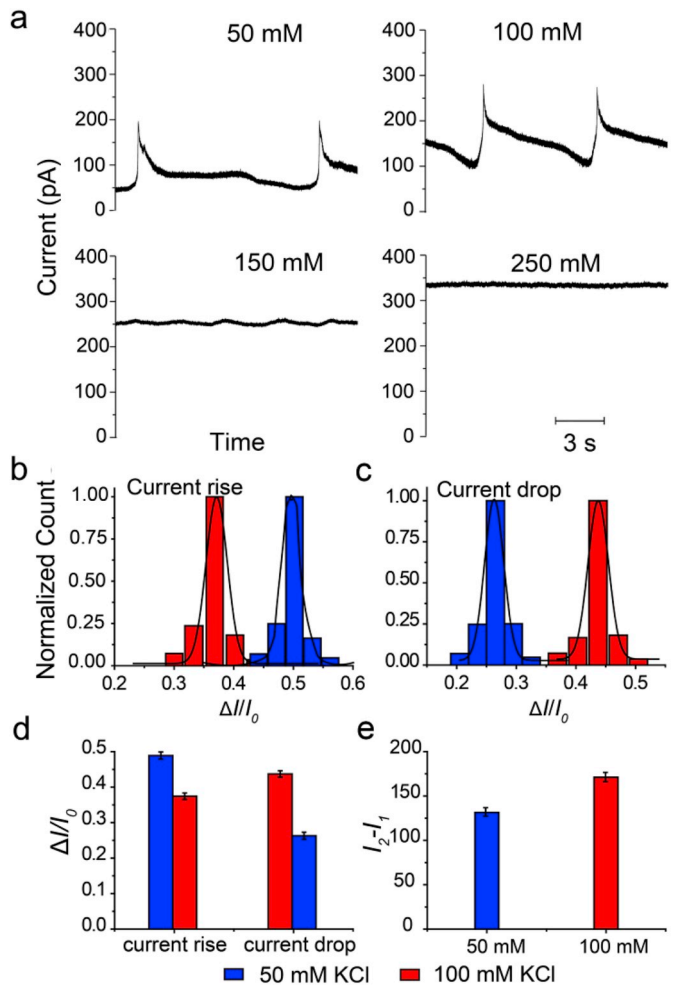

Fig. 5. (a) Typical current-time traces for lysozyme translocation at different salt concentrations of 50 mM, 100 mM, 150 mM and 250 mM. The experiments were conducted in KCl (buffered at pH 7.0), at a voltage of +1000 mV with 100 nM lysozyme in base side chamber. The normalized histograms of current changes ($\Delta I/I_0$) of a total of 267 translocation events: current rise (b) and drop (c) at 50 mM (blue) and 100 mM (red), respectively. (d) Effect of the salt concentrations on the normalized current change ($\Delta I/I_0$) at 50 mM (blue) and 100 mM (red), respectively. (e) The current change ($I_2 - I_1$) at 50 mM (blue) and 100 mM (red), respectively. (For interpretation of the references to color in this figure legend, the reader is referred to the Web version of this article.)

particles were voltage dependent and more pronounced at higher voltages (Lan et al., 2014). Therefore, $\Delta I_2/I_0$ enhanced with the increase of voltage from 800 mV to 1000 mV. For $\Delta I_1/I_0$, it also increased with the voltage increasing, similar result was also seen for particles passing through a glass pipets at lower salt concentrations (Qiu et al., 2016b). Furthermore, with the voltage decreasing from +1000 mV to +800 mV, the time interval (τ_{on}) and dwell time (τ_{off}) of individual event are prolonged due to the decreased driving force (Fig. 4d and e), and the detail data of the normalized histograms for τ_{on} and τ_{off} were shown in Figs. S6c and d. As for no signals were observed at + 700 mV, a possible explanation can be that the electrical field driving force was insufficient to make the lysozyme transport through the nanochannel at this voltage.

The salt concentration dependence experiments of lysozyme translocation through the nanochannel were carried out in a range of KCl concentrations, as shown in Fig. 5a. It was found that as the KCl concentration decreased from 100 mM to 50 mM, $\Delta I_2/I_0$ increased from 0.374 ± 0.001 to 0.489 ± 0.001, while $\Delta I_1/I_0$ decreased from 0.437 ± 0.001 to 0.263 ± 0.001 by analysing a total of 267 translocation events (Fig. 5b and c). However, with KCl concentration increasing to 150 mM, biphasic pulses were less evident and even no current signal was detected when the electrolyte concentration reached 250 mM. These results indicated that the surface charge effect became more prominent and governed the shape of biphasic pulse at low KCl concentration. Nevertheless, the electrical double layers associated with the nanochannel and the charged lysozyme were screened at higher KCl concentration (Lan et al., 2014; Weatherall and Willmott, 2015), thus the Debye length became shorter, leading to the increase of the effective diameter of the nanochannel as well as the decrease of the lysozyme-nanochannel electrostatic interactions. Taking together, the combined actions of all factors make biphasic pulse insignificant or be eliminated at higher electrolyte concentration. Furthermore, Lan et al. have also been reported that the surface charge effect on nanoparticle translocation could be eliminated by the increase of electrolyte concentration. In short, the biphasic pulse waveshape (Fig. 5a) and signal-to-noise ratio (Fig. 5d and e) are presented well at the KCl concentration 100 mM.

3.3. Detection of lysozyme

Since the translocation of lysozyme could result in characteristic biphasic pulses, the present nanochannel offers the potential to develop high-precision sensing device for lysozyme. To testify this concept,

lysozyme at various concentrations were examined under the optimum conditions (100 mM KCl, 10 mM Tris-HCl at pH 7.0, with the transmembrane potential of +1000 mV). As displayed in Fig. 6a, the frequency of biphasic pulses increased with an increase in the concentration of lysozyme. Linear regression analysis showed good linearity between the biphasic pulses frequency and the lysozyme concentration ranging from 10 nM to 400 nM with a correlation coefficient of 0.998 (Fig. 6b). The linear regression equation was Freq = 0.08421x + 0.4013 (x is lysozyme concentration). The detection limit was estimated to be 1.2 nM in about 30 min electrical recording. A comparison of various techniques for lysozyme detection was summarized in Table S2, the performance of the biosensor is comparable with those of sensitive SPR, fluorescence and phosphorescence. Although the detection limit of our biosensor is higher than some reported electrochemical assays, it was free of labeling procedure as well as extra sophisticated signal amplification strategy such as AuNPs networks or hybridization chain reaction (HCR). Moreover, simplicity, rapid and single-molecule resolution are the motivating factors of the proposed biosensor. To evaluate the reproducibility of our approach, three different concentrations of lysozyme including 10 nM, 50 nM and 100 nM were repeatedly measured (Table S3). The results showed that the coefficients of variation (CVs) of the intra-assay were 1.68%, 1.26% and 1.01% (n = 3), while the CVs of the inter-assay with various batches were 2.38%, 1.41% and 1.04% (n = 3), respectively, indicating acceptable precision and satisfactory reproducibility of the biosensor.

To investigate the selectivity of the nanodevice for lysozyme detection, trypsin (MW 23.3 kDa, pI 10.1) as a representative interfering substance was investigated due to its similar molecular weight and isoelectric point to lysozyme. The interference experiments were conducted in 100 mM KCl (10 mM Tris-HCl, pH 7.0) at an applied potential of +1000 mV. As shown in Fig. 6c, no translocation signal was observed for 100 nM trypsin. For the protein mixtures of lysozyme and trypsin, only the biphasic pulse signals of lysozyme were generated (Fig. 6d), which is the same as that of only lysozyme. However, the signals of the sequential addition (first trypsin, then lysozyme) are different: after adding lysozyme in the trypsin solution, there are short-life irregular signals be produced before generating the normal biphasic pulses of lysozyme (Fig. 6e). These signals should be ascribed to the weak adsorption of trypsin molecules and the replacement of lysozyme for the adsorbed trypsin due to the stronger electrostatic attraction between the lysozyme and the inner wall. Except for trypsin, we also tested BSA and HSA under 100 mM KCl (10 mM Tris-HCl, pH 7.0), and did not observed their biphasic pulse signals and the effects on lysozyme signals (Fig. S7). This could be originated from the negative charges on BSA and HSA molecules.

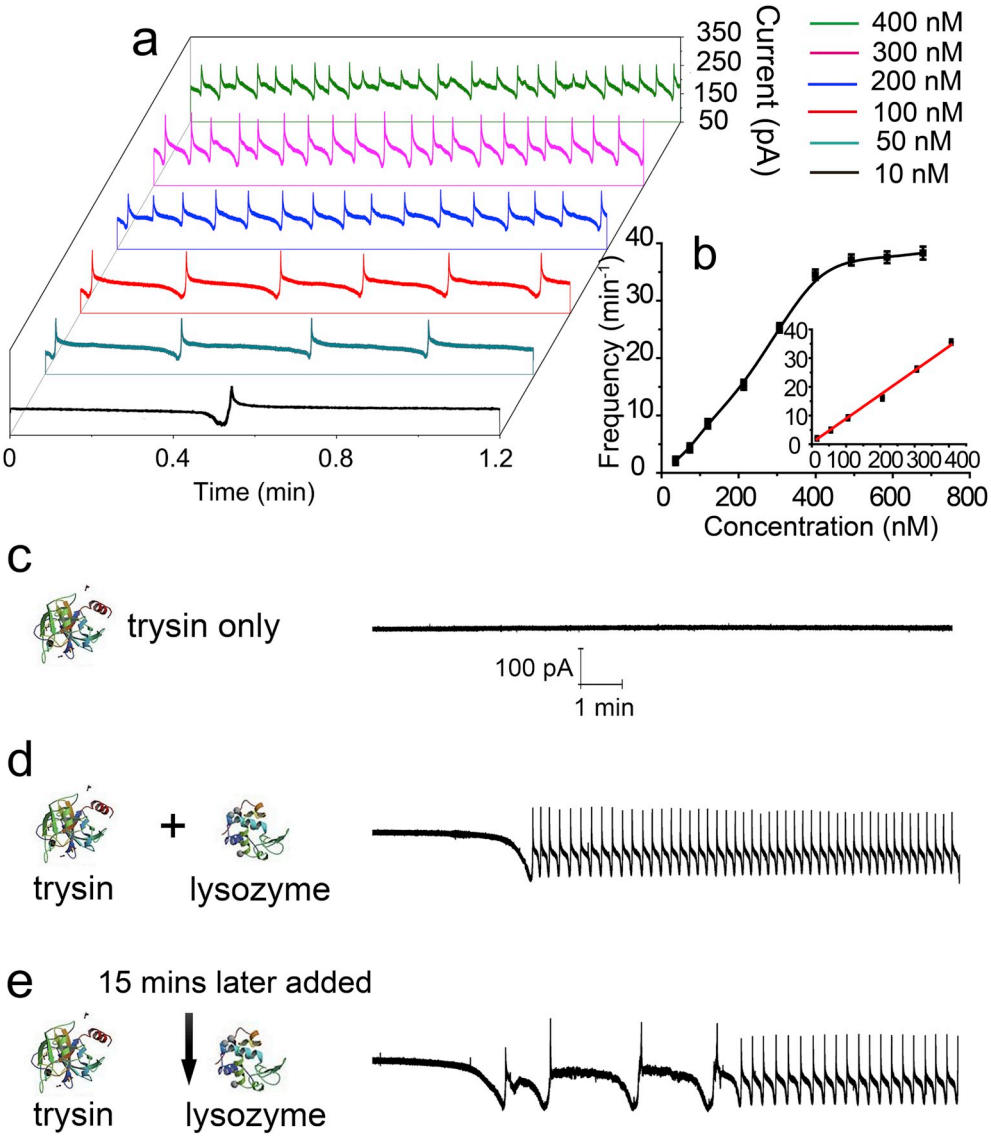

Fig. 6. (a) Biphasic pulses current traces acquired in different concentrations of lysozyme recordings ranging from 10 nM to 400 nM. (b) The linear correlation between the frequencies of the transport events and the concentrations of lysozyme. Typical current-time traces separately tested in 100 nM trypsin solution (c), the mixture solution of 100 nM trypsin and 100 nM lysozyme (d). (e) The mixture solution of 100 nM lysozyme and 100 nM trypsin, according to the way of succedent addition of 100 nM lysozyme to 100 nM trypsin solution denoted in (c) after 15 min testing.

4. Conclusions

In summary, we have successfully constructed a biphasic-pulse nanopore biosensor and applied in the sensitive detection of lysozyme. The generation, regulation and mechanism of biphasic pulse signals are systemically investigated in PET nanopore by using lysozyme as a translocating molecule. The promising approach allowed rapid and label-free detecting of lysozyme with a low detection limit of 1.2 nM and the whole sensing process can be achieved within 30 min. The proposed biosensor as a detector possesses the advantages of high sensitivity and selectivity due to good signal-to-noise ratio, the resolution and signal reproducibility. Such capability is particularly relevant to biological applications that rely on detection of minute concentrations of analytes in small volumes or even in complex biofluids. Future studies will focus on exploring the underlying mechanism of the biphasic-pulse signals, and improve its anti-interference ability in complex matrix. The biphasic-pulse nanodevice is expected to be applied to sense other small biomolecules, and have promise to construct IED used in disease prediction and diagnosis.

Declaration of competing interest

The authors declare that they have no known competing financial interests or personal relationships that could have appeared to influence the work reported in this paper.

CRediT authorship contribution statement

Hong Sun: Methodology, Writing - original draft. **Fujun Yao:** Methodology, Writing - review & editing. **Xiao-Feng Kang:** Writing - review & editing, Supervision.

Acknowledgments

This work was financially supported by the National Natural Science Foundation of China (Grants 21375104, 21327806 and 21874107), and Natural Science Basic Research Plan in Shaanxi Province of China (Grant 2016JQ2021).

Appendix A. Supplementary data

Supplementary data to this article can be found online at https://doi.org/10.1016/j.bios.2019.111740.

References

Anderson, B.N., Muthukumar, M., Meller, A., 2013. ACS Nano 7, 1408–1414.
Arnott, P.M., Howorka, S., 2019. ACS Nano 13, 3334–3340.
Bayley, H., Martin, C.R., 2000. Chem. Rev. 100, 2575–2594.
Chang, H., Kosari, F., Andreadakis, G., Alam, M.A., Vasmatzis, G., Bashir, R., 2004. Nano Lett. 4, 1551–1556.
Chen, K., Shan, L., He, S., Hu, G., Meng, Y., Tian, Y., 2015. J. Phys. Chem. C 119, 8329–8335.
Cheng, A., Tereshchenko, L.G., 2011. J. Electrocardiol. 44, 611–615.
Ding, D., Gao, P., Ma, Q., Wang, D., Xia, F., 2019. Small, 1804878.
Dong, Y., Cheng, Y., Xu, G., Cheng, H., Huang, K., Duan, J., Mo, D., Zeng, J., Bai, J., Sun, Y., Liu, J., Yao, H., 2019. ACS Appl. Mater. Interfaces 11, 14960–14969.
Fanzio, P., Mussi, V., Menotta, M., Firpo, G., Repetto, L., Guida, P., Angeli, E., Magnani, M., Valbusa, U., 2015. Biosens. Bioelectron. 64, 219–226.
Farimani, A.B., Dibaeinia, P., Aluru, N.R., 2017. ACS Appl. Mater. Interfaces 9, 92–100.
Feiner, R., Dvir, T., 2018. Nat. Rev. Mater. 3, 17076.
Garaj, S., Hubbard, W., Reina, A., Kong, J., Branton, D., Golovchenko, J.A., 2010. Nature 467, 190–193.
Harrell, C.C., Choi, Y., Horne, L.P., Baker, L.A., Siwy, Z.S., Martin, C.R., 2006. Langmuir 22, 10837–10843.
Haselberg, R., Harmsen, S., Dolman, M.E.M., de Jong, G.J., Kok, R.J., Somsen, G.W., 2011. Anal. Chim. Acta 698, 77–83.
Houghtaling, J., List, J., Mayer, M., 2018. Small 14, 18024112.
Kang, X.-F., Cheley, S., Guan, X., Bayley, H., 2006. J. Am. Chem. Soc. 128, 10684–10685.
Kim, S.J., Cho, K.W., Cho, H.R., Wang, L., Park, S.Y., Lee, S.E., Hyeon, T., Lu, N., Choi, S. H., Kim, D.-H., 2016. Adv. Funct. Mater. 26, 3207–3217.
Kwak, D.-K., Chae, H., Lee, M.-K., Ha, J.-H., Goyal, G., Kim, M.J., Kim, K.-B., Chi, S.-W., 2016. Angew. Chem. Int. Edit. 55, 5713–5717.
Lan, W.-J., Kubeil, C., Xiong, J.-W., Bund, A., White, H.S., 2014. J. Phys. Chem. C 118, 2726–2734.
Lin, X., Ivanov, A.P., Edel, J.B., 2017. Chem. Sci. 8, 3905–3912.
Manrao, E.A., Derrington, I.M., Laszlo, A.H., Langford, K.W., Hopper, M.K., Gillgren, N., Pavlenok, M., Niederweis, M., Gundlach, J.H., 2012. Nat. Biotechnol. 30, 349–353.
Migliore, F., Viani, S., Bongiorni, M.G., Zorzi, A., Silvetti, M.S., Francia, P., D'Onofrio, A., De Franceschi, P., Sala, S., Donzelli, S., Ricciardi, G., Menardi, E., Giammaria, M., La Greca, C., Bauce, B., Rigato, I., Iliceto, S., Bertaglia, E., Diemberger, I., Corrado, D., 2019. Int. J. Cardiol. 280, 74–79.
Mossesso, V.N., Li, J., Landsittel, D., Ganz, L.I., 2011. Circulation 124.
Qiu, Y., Lin, C.-Y., Hinkle, P., Plett, T.S., Yang, C., Chacko, J.V., Digman, M.A., Yeh, L.-H., Hsu, J.-P., Siwy, Z.S., 2016. ACS Nano 10, 8413–8422.
Qiu, Y., Vlassiouk, I., Chen, Y., Siwy, Z.S., 2016. Anal. Chem. 88, 4917–4925.
Rezaei, B., Jamei, H.R., Ensafi, A.A., 2018. Biosens. Bioelectron. 115, 37–44.
Sexton, L.T., Mukaibo, H., Katira, P., Hess, H., Sherrill, S.A., Horne, L.P., Martin, C.R., 2010. J. Am. Chem. Soc. 132, 6755–6763.
Siwy, Z.S., Howorka, S., 2010. Chem. Soc. Rev. 39, 1115–1132.
Smeets, R.M.M., Keyser, U.F., Krapf, D., Wu, M.Y., Dekker, N.H., Dekker, C., 2006. Nano Lett. 6, 89–95.
Steinbock, L.J., Krishnan, S., Bulushev, R.D., Borgeaud, S., Blokesch, M., Feletti, L., Radenovic, A., 2014. Nanoscale 6, 14380–14387.
Thakur, A.K., Movileanu, L., 2019. Nat. Biotechnol. 37, 96–101.
Van Meervelt, V., Soskine, M., Singh, S., Schuurman-Wolters, G.K., Wijma, H.J., Poolman, B., Maglia, G., 2017. J. Am. Chem. Soc. 139, 18640–18646.
Verschueren, D.V., Pud, S., Shi, X., De Angelis, L., Kuipers, L., Dekker, C., 2019. ACS Nano 13, 61–70.
Wang, C., Fu, Q., Wang, X., Kong, D., Sheng, Q., Wang, Y., Chen, Q., Xue, J., 2015. Anal. Chem. 87, 8227–8233.
Weatherall, E., Willmott, G.R., 2015. J. Phys. Chem. B 119, 5328–5335.
Wei, K., Yao, F., Kang, X.-F., 2018. Biosens. Bioelectron. 109, 272–278.
Xiao, K., Wen, L., Jiang, L., 2016. Small 12, 2810–2831.
Yadav, I., Kumar, S., Aswal, V.K., Kohlbrecher, J., 2017. Langmuir 33, 1227–1238.
Ying, Y.-L., Hu, Y.-X., Gao, R., Yu, R.-J., Gu, Z., Lee, L.P., Long, Y.-T., 2018. J. Am. Chem. Soc. 140, 5385–5392.
Yu, R.-J., Ying, Y.-L., Gao, R., Long, Y.-T., 2019. Angew. Chem. Int. Edit. 58, 3706–3714.
Zhao, C., Li, X., Li, L., Gong, X., Chang, Y., Zheng, J., 2013. Chem. Commun. 49, 9317–9319.
Zheng, Q., Zhang, H., Shi, B., Xue, X., Liu, Z., Jin, Y., Ma, Y., Zou, Y., Wang, X., An, Z., Tang, W., Zhang, W., Yang, F., Liu, Y., Lang, X., Xu, Z., Li, Z., Wang, Z.L., 2016. ACS Nano 10, 6510–6518.
Zhou, Y.F., Morais-Cabral, J.H., Kaufman, A., MacKinnon, R., 2001. Nature 414, 43–48.